Article

Journal of
Nanoscience and Nanotechnology
Vol. 20, 1–7, 2020
www.aspbs.com/jnn

Localized Surface Plasmon Resonance Studies on Pd/C Nano-Composite System: Effect of Metal Concentration and Annealing Temperature

P. K. Kulriya[1,*], V. N. Singh[2], D. C. Agarwal[3], S. Ojha[1], and D. K. Avasthi[4]

[1] *Materials Science Group, Inter-University Accelerator Centre, New Delhi 110067, India*
[2] *Council of Scientific and Industrial Research (CSIR)-National Physical Laboratory, Dr. K. S. Krishnan Marg, New Delhi 110012, India*
[3] *Sant Longowal Institute of Engineering and Technology, Sangrur, Longowal 148106, Punjab, India*
[4] *Amity Institute of Nanotechnology, Amity University, Noida 201313, India*

The effects of metal concentration and annealing temperature on the localized surface plasmon resonance (LSPR) properties of the Pd nanoparticles (NP) dispersed in carbon were investigated. The Pd/C nano-composite thin films with 7 to 39 atomic % concentration of metal content were deposited using the atom beam co-sputtering techniques and subjected to annealing at temperature varying from 300 °C to 600 °C. The UV-vis spectroscopy studies on as-prepared films displayed a Mie scattering profile, but not well-defined LSPR bands were observed for all the values of Pd concentration. This is attributed to the smaller size (3–4 nm) of Pd NPs and rough Pd/C interface, as confirmed from TEM studies. When samples were annealed at a temperature of 300 °C, three broad LSPR absorption bands in the visible region, along with a sharp peak at 210 nm, were observed and the effect of Pd concentration variation was insignificant on their position. The multiple LSPR bands were observed due to agglomeration NPs, which is consistent with earlier reports and is also observed in the TEM images. When annealing temperature was subsequently increased to 500 °C, a blue shift in the LSPR peak position with an increase in the Pd concentration was observed, which phenomena is attributed to the formation of bigger NPs with the formation of sharp NPs-interface at high temperature upon annealing. A monotonic increase in the magnitude and decrease in the FWHM with an increase in concentration suggested change in the dielectric function of sample due to the growth of NPs. This is further confirmed from XRD studies, where strain relaxation and grain growth were observed. The intensity of the SPR peak decreased with an increase in the annealing temperature. The LSPR peak disappeared on annealing at a temperature of 600 °C, suggesting the formation of continuous polycrystalline thin films of Pd. In summary, NPs size, metal-matrix interface, and concentration of metal play key roles in the tailoring the LSPR properties of the Pd.

Keywords: Nano-Composite, Surface Plasmon Response, Annealing Temperature.

1. INTRODUCTION

The surface plasmonic properties of nanostructure metals have stimulated considerable interest because of their applications in diverse fields such as optical sensing of biomolecules, photothermal therapy, spectral signal enhancement, photovoltaic conversion efficiency enhancement, optical waveguide, and monitoring of catalytic reactions [1]. Among all metals, noble metal nanoparticles (NP) have closely spaced conduction and valence bands which assist in the induction of localized surface plasmon resonance (LSPR) by coherent oscillation of free-electrons on the metal surface [2]. The LSPR generates very strong local fields at the interface which can be tuned by controlling NP size, size distribution, shape, morphology, surrounding media, and its composition [3–6]. The LSPR in Au NPs was schematically tuned from the visible to the near-infrared range by controlling size and morphology of the nanostructure [7–8]. Recently, numerous efforts have been made to tailor the LSPR

*Author to whom correspondence should be addressed.
†Present address: Materials Science Group, Inter-University Accelerator Centre, New Delhi 110067, India.

properties of nanostructured palladium (Pd) that exhibits various physical properties similar to other noble metal (Au, Ag, Cu). However, bulk Pd is not considered to be a promising candidate for LSPR properties, due to its peculiar dielectric function and because the position of its LSPR peak lies in the ultraviolet spectral range as a result of the strong coupling between plasmon transition and the inter-band excitation [9]. A tuneable LSPR peak in the near-infrared region was displayed by the freestanding hexagonal Pd nanosheets of thickness <10 atomic layers [1]. The SPR features of nanostructure Pd were not detected in the visible and near infrared regions for NPs of size <10 nm [10]. The calculation performed using Mie theory suggested that the position of the SPR peak for smaller size (<10 nm) Pd NPs lies below 250 nm [11]. Pd nanoplates of 45 nm edge length exhibited red shift in the LSPR peaks to the visible region (up to 610 nm) [12]. The LSPR peak for Pd nano-cubes having a size of >25 nm was observed in the visible region at nearly the same location (∼ 400 nm) as that of Ag and Au NPs [10]. The width of the LSPR band strongly depends upon the shape of the NPs, and a very broad LSPR peak over the entire visible region was reported for star shaped Pd NPs [13]. The triangular and hexagonal shaped Pd nanoplates exhibited LSPR peaks at 520 nm and 530 nm, respectively [14]. The corrosion based synthesis of Pd nano-cube showed tuning the LSPR peak from 410 nm to 530 nm by varying wall thickness of the cube [15]. The LSPR peak for Pd–Ag alloy NPs was tuned across the entire visible spectrum from 440 to 730 nm by changing the interfacial chemistry by varying the composition of the Pd and Ag [16]. Kundu et al. observed a broad LSPR band in the range 330–480 nm for Pd nanocubes [17]. The hexagonal Pd nanosheets with different edge lengths (6.4 to 59.2 nm) exhibited a tuneable LSPR in the range of 820–1067 nm [18]. The theoretical calculations performed using the discrete dipole approximation (DDA) method showed that the LSPR features of Pd can be tailored from the ultra-violet (330 nm) to the visible (530 nm) region by controlling the shape of NPs from cube to triangular [19–21]. In summary, most of the reported results on Pd NPs samples have been synthesized by chemical techniques using toxic gas (i.e., CO) as reducing and capping agents during the synthesis process. There is a strong possibility of impurities developing and degradation of the NPs occurring due to exposure to the external atmosphere.

In this study, Pd NPs embedded in carbon matrix have been deposited using physical deposition process in the vacuum system. The NPs were embedded in carbon to help protect the NPs from oxidation and also make them well-separated. The effect of metal concentration and annealing temperature on the LSPR response of the Pd NPs is investigated. The observation of a strong optical absorption band in the visible region on annealing of Pd NPs embedded in carbon matrix is explained within the framework of Mie scattering theory.

2. EXPERIMENTAL DETAILS

Pd NPs embedded in the carbon matrix were deposited on quartz and glass substrates using co-sputtering of high purity Pd (99.99%) and graphite target by an atom beam sputtering setup equipped with a 1.5 keV Ar atoms [22–24]. The sputtering target was a 2 mm thick graphite disc of 50 mm diameter on which 0.2 mm thick Pd foils of 3×3 mm^2 were symmetrically glued. The base pressure in the sputtering chamber before the deposition was 2.0×10^{-6} mbar. Sputtering was carried out at an ion beam current of 14.8 mA with a slow deposition rate of 8–10 nm/h in Ar gas pressure of 1.5×10^{-3} mbar. Three sets of as-prepared Pd NPs having Pd concentration ∼5, 20 and 40 atomic percentage in the host matrix (represented as AC5, AC20, and AC40, respectively) have been used in this study. The annealing of as-prepared samples was performed in Ar atmosphere from 300 °C to 600 °C for a duration of 1 h. As-prepared and annealed samples were characterized by Rutherford backscattering spectrometry (RBS), glancing angle x-ray diffraction (GAXRD), high-resolution transmission electron microscopy (HRTEM), selected area electron diffraction (SAED), energy dispersive x-ray spectroscopy (EDX), micro-Raman and UV-visible absorption spectroscopy techniques. The composition of the nano-composite thin films was estimated using RBS and EDX techniques. The RBS measurements (normal incidence to the sample surface with a collection of the backscattered ions at an angle of 170°) were carried out using a 1.7 MV Pelletron accelerator at the Inter-University Accelerator Centre (IUAC), New Delhi, India. The microstructure of the Pd NPs films deposited on Carbon coated Cu TEM grids were determined using a Technai G20-stwin HRTEM operated at 200 kV. Structural analysis is carried out using SAED patterns and a Bruker AXS D8 advanced glancing X-ray diffractometer equipped with a Cu x-ray tube (wavelength: 1.5405 Å), Göble mirror, and scintillator detector. The SPR behaviors of films deposited on quartz substrates were recorded using a dual-beam U-3300 Hitachi spectrometer. A Renishaw in-Via micro-Raman microscope equipped with Ar ion laser (514 nm excitation, 10 mW power, 20× objective) was used for short ranging structural ordering in the sample.

3. RESULTS AND DISCUSSION

The concentration of AC5, AC20, and AC40 samples were measured using RBS spectrometer, and the estimated values of the Pd concentration in Carbon matrix were 7, 24 and 39 atomic %, respectively. The UV-vis absorbance spectroscopy studies were performed with the aim to investigate the effect of NP concentration and annealing temperature on the LSPR properties of the Pd nanoparticle embedded in carbon matrix. Figure 1 shows the UV-vis absorbance spectra of AC5 sample as prepared and as annealed at temperatures of 300 °C, 400 °C, 500 °C, and

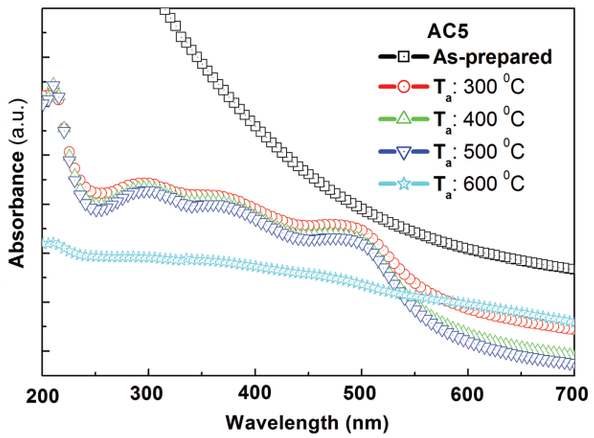

Figure 1. UV-vis absorbance spectrums of the sample AC5 as prepared and as annealed at various temperatures of 300 °C, 400 °C, 500 °C, and 600 °C. Four absorption peaks are found in the spectrum: A sharp peak at 210 nm, a broad absorption band centred on 296 nm, 375 nm, and 500 nm on annealing performed at the temperature of 300 °C.

600 °C. In case of the as-prepared sample, the absorption profile did not show a well-defined surface-plasmon band; instead. On annealing at temperature of 300 °C, three characteristic absorption bands (296 nm, 375 nm and 500 nm), along with a sharp peak (210 nm), were observed. The variation in the peak positions with annealing temperature and Pd concentration are reported in Table I. It may be noted that the positions of all bands were in the visible region of the spectrum. When annealing temperature was increased to 400 °C, the positions of bands at lower wavelength 296 nm and 375 nm remained unchanged, whereas the position of the band appearing at higher wavelength shifted from the wavelength of 500 nm to 487 nm. When the annealing temperature was further increased to 500 °C, the position of the absorption bands remained unchanged, but the intensity of absorbance at higher wavelengths decreased. The LSPR peaks disappeared when the sample was subjected to further annealing at a temperature of 600 °C. Figure 2 shows the UV-vis absorbance spectra of the AC20 sample as prepared as well as annealed at temperatures of 300 °C, 400 °C, 500 °C, and 600 °C. Similar to the AC5 sample, three absorbance bands and a sharp peak at around 210 nm were observed. It may be noted that the position of the bands in both samples annealed at same temperature (300 °C) are identical. When temperature was increased to 400 °C, the position of the absorbance band at 296 nm remained the same, while the position of the absorbance bands at 375 nm and 500 nm shifted by 5 nm and 15 nm, respectively. Upon comparing the results of AC5 and AC20 samples, it is clear that there is a blue shift in the position of both the bands at 375 nm and 500 nm with an increase in the concentration. The position of these bands remained unchanged when the annealing temperature was increased to 500 °C. When temperature was further increased to 600 °C, no absorbance peak was observed. Figure 3 shows the UV-vis absorbance spectrum of the AC40 sample as prepared and as annealed at temperatures of 300 °C, 400 °C, 500 °C, and 600 °C. In the as-prepared sample, absorbance peaks were not observed. When the sample was subjected to annealing at 300 °C, three absorbance bands and one sharp peak were observed, and the results were similar to the results for the lower concentration AC5 and AC20 samples. When the annealing temperature was further increased to 400 °C, the position of the absorption band at 296 nm remained unchanged, but the position of the absorbance bands at 375 nm and 500 nm shifted by ∼9 nm and ∼22 nm respectively. This displays a large blue shift in the position of both absorption bands (375 nm and 500 nm) when concentration was increased. The effect of higher annealing temperature (500 °C and 600 °C) on the LSPR bands of AC40 sample is similar to that of the AC5 and AC20 samples. For a better evaluation of the effects of Pd concentration on the SPR peak position, a representative plot of AC5, AC20, and AC40 samples annealed at 500 °C is shown in Figure 4. It clearly shows that the intensity of the LSPR bands is increasing with an increase in the concentration of the Pd in the carbon matrix. Three broad absorbance bands (296 nm, 375 nm, and 500 nm) in visible region and a sharp peak at 210 nm were observed for all concentrations of Pd. As the concentration was increased from 7 atomic % to 39 atomic % the position of the LSPR bands at 296 nm and 210 nm was not affected, but blue shifts were observed for the bands at 375 nm and 500 nm.

Table I. The effect of concentration and annealing temperature on the SPR peak position of the Pd nanoparticle embedded in carbon matrix.

		300 °C	400 °C	500 °C	600 °C
Sample code	As-prepared	Shift in the position of absorption band w.r.t to AC40			
AC5	No band in visible region	0	0	0	No band in visible region
		0	0	0	
		0	(−)13	(−)13	
AC20		0	0	0	
		0	(−)5	(−)5	
		0	(−)15	(−)15	
AC40		0	0	0	
		0	(−)9	(−)9	
		0	(−)22	(−)22	

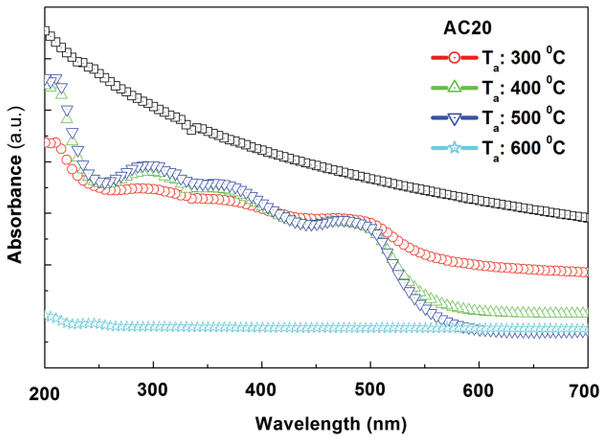

Figure 2. UV-vis absorbance spectrums of sample AC20 as prepared and as annealed at various temperatures of 300 °C, 400 °C, 500 °C, and 600 °C.

To investigate the role of size, and Pd/C interface on the SPR properties, the structural studies on the as-prepared and annealed AC40 sample were performed using TEM, SEAD, and XRD. Figure 5 shows the TEM images for (a) as-prepared and (b) magnified image of the AC40. The SAED pattern of the AC40 sample shown as the inset of the Figure 5(a). The magnified TEM image also revealed that NPs had a rough surface and the Pd/C interface was not sharp. It shows that Pd NPs were uniformly distributed across the sample and that the average size was about 3 nm. The inset is the SAED pattern Figure 5(a) of Pd NP confirmed the polycrystalline fcc structure of Pd. Figure 6 displays the TEM images of the Pd NPs annealed at (a) 300 °C, (b) 400 °C, and (c) 500 °C. The TEM image of the AC40 sample annealed at 300 °C exhibited percolated structures constructed by agglomeration and combination of smaller nano-particles. Some NPs having size larger than the as-deposited sample can be also seen in

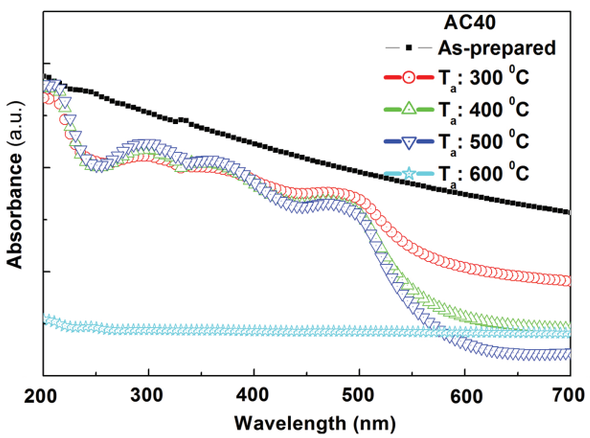

Figure 3. UV-vis absorbance spectrums of the AC40 sample as prepared and as annealed at various temperature of 300 °C, 400 °C, 500 °C, and 600 °C.

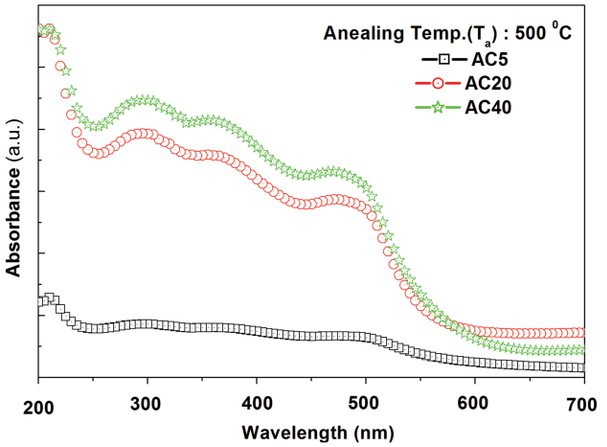

Figure 4. UV-vis absorbance spectrums of the AC5, AC20, and AC40 samples annealed at temperature of 500 °C. It displays a blue shift of 22 nm in the LSPR peak position with the change in concentration. The magnitude of the LSPR peak increased and the width decreased with an increase in the Pd concentration.

Figure 6(a). It may be noted that the NPs were not in the perfect spherical shape upon annealing. The SAED pattern, as shown in the inset of Figure 6(a), exhibited brighter diffraction rings with a few spots, indicating the improvement in the crystallinity of Pd upon high temperature annealing. When the annealing temperature was further increased to 400 °C (Fig. 6(b)), a binomial distribution in the size of the NPs was observed. The average size $\langle D \rangle$ for the smaller NPs was $\sim$ 4–5 nm, whereas the size of the larger NPs was about 100 nm. It shows that the size of the smaller NPs was almost equivalent to the size of the as-deposited NPs, whereas few larger-sized NPs grew due to annealing. It may also be noted that the density of smaller-sized NPs is higher than larger-sized particles. The effect of even further annealing at the temperature of 500 °C is revealed by the TEM images in Figure 6(c).

It can be clearly seen from figure that the density of bigger-sized NPs increased in comparison to smaller-sized NPs, but the change in the size was insignificant. It may be noted that the shapes of the NPs also changed from spherical to polyhedral. The observation of large number of spots in the SAED pattern indicated that a few of polycrys-

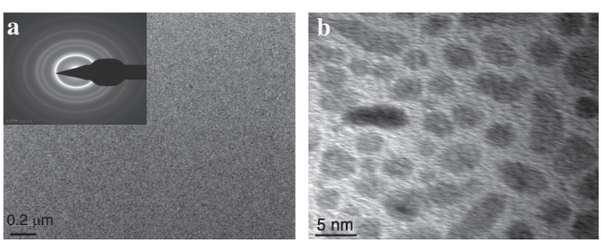

Figure 5. TEM images of (a) as-deposited Pd NPs in carbon matrix and (b) magnified image showing uniformly-distributed Pd NPs. The SAED pattern (inset) of individual NPs confirming its polycrystalline structure.

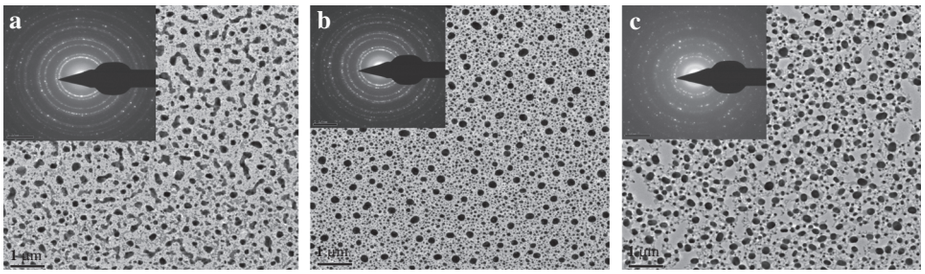

Figure 6. Effect of variation in annealing temperature such as (a) 300 °C, (b) 400 °C, and (c) 500 °C on the microstructure of the Pd/a-C nanocomposite thin films. SAED patterns for annealed films are shown in the inset of each figure.

talline Pd NPs grew to larger particles of Pd. The effect of annealing temperature on the structural properties is further investigated by XRD. Figure 7 displays XRD pattern of the as-prepared AC40 sample and as treated at temperatures of 300 °C, 400 °C, 500 °C and 600 °C. The peaks can be readily indexed to face-centred cubic Pd phase (JCPDS file No 46-1043). The average crystalline size estimated from the Scherrer formula varies from 7.7 nm to 11.6 nm with the increase in annealing temperature from 300 °C to 600 °C. It can also be seen that the crystallinity of film improved with the increase in the annealing temperature. The calculated value of micro-strain changed from 1.73% in as-deposited NPs to 0.09% for the sample annealed at 600 °C. The crystalline size and micro-strain parameters are reported in the Table II. The micro-strain relaxation upon annealing can be attributed to the increase in size of NPs upon annealing. It may be noted that the value of strain for the sample annealed at 600 °C was negligible, indicating that NPs got agglomerated and formed a continuous film. The effect of concentration on the microstructure has already been reported elsewhere [23], where the increase in NP size with increase in the concentration of Pd in the carbon matrix has been shown.

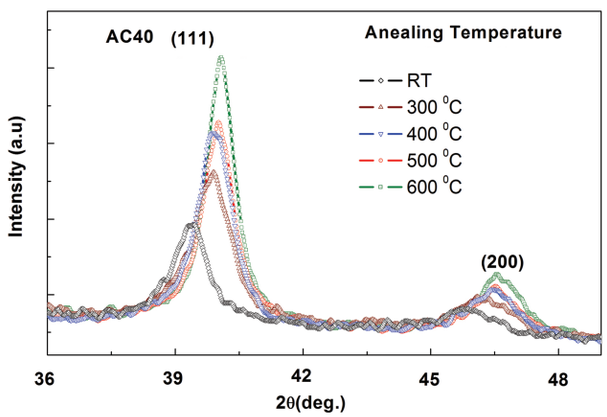

Figure 7. GAXRD pattern of the AC40 sample annealed at 300 °C, 400 °C, 500 °C, and 600 °C, recorded at glancing angle 2°. The strain induced by the matrix was relaxed on annealing. The increase in intensity of Pd (111) peak indicated improvement in crystallinity upon annealing.

It has been reported that the distance between metal NPs, aggregate size, polarization direction, shape, and surrounding matrix significantly influence the position, width, shape, and intensity of the LSPR peak [25]. The LSPR for metal NPs embedded in dielectric matrix was explained using the interface effect, where electrons were confined at the interface between the metal and the surrounding dielectric and get excited resonantly by an incident electromagnetic wave, which results in the LSPR [2–3]. In the present study, experimental results of as-prepared samples showed that the absorbance does not show well-defined LSPR bands. A similar profile was also reported for the alkanethiolate-protected Pd NPs [26]. The LSPR peak in the as-prepared sample is not observed in present case due to the too small size of NPs (∼3 nm) and rough Pd/C interface, which is expected to give a LSPR peak only in the far ultra-violet region, as reported by earlier investigations [10]. Upon annealing, three broad bands in the visible range and a sharp peak at 201 nm appeared. The LSPR peak at 210 nm was due to an improvement in the crystallinity and growth in the NPs size. A broad absorbance band centred at 590 nm in the visible region with a sharp peak at 210 nm was also observed in the N-vinyl pyrolidone stabilized Pd nano-spheres ($D \sim 10$ nm and 100 nm), and the effect was attributed to the polycrystalline and peculiar dielectric function of the Pd [27]. The appearance of two humps in the SPR spectrum in the range 250–330 nm for the cubical shape Pd NPs has been reported [17]. The multiple humps appeared due to the formation of anisotropic NPs owing to agglomeration of smaller NPs upon annealing, which can be clearly seen in the TEM images Figure 6(a). In agglomerated NPs,

Table II. Calculated values of strain and crystalline size as prepared and as annealed at different temperatures for sample AC40.

AC40	2θ (deg)	PFWHM (deg)	Crystalline size (nm)	$\langle d \rangle$ Å	Strain (%)
As-prepared	39.40	0.88	7.7	2.285	1.73
$T = 300$ °C	39.80	0.81	8.3	2.263	0.75
$T = 400$ °C	39.91	0.67	10.1	2.257	0.49
$T = 500$ °C	40.01	0.63	10.7	2.251	0.22
$T = 600$ °C	40.07	0.58	11.6	2.248	0.09

oscillating electrons in one particle experience the electric field due to the oscillations in the neighbouring particle, which leads to a collective plasmon oscillation of the aggregated system that gives an additional peak in the SPR spectrum [28].

In the present study, Pd NPs were dispersed in the carbon matrix; therefore, the wide absorbance band can be attributed to the combined effect of the dielectric function of Pd and carbon. The concentration-dependent LSPR studies showed increase in the magnitude of the band and a decrease in the width with an increase in the Pd concentration in the carbon matrix. The expression for calculating the FWHM of the LSPR peak ($\Delta\lambda$) can be determined by using an improved Mie theory [29].

$$d = \frac{v_f \lambda_p^2}{2\pi c \Delta\lambda} \quad (1)$$

Where, c is velocity of light, and λ_p is the wavelength of LSPR peak which depends on the dielectric of carbon and the concentration of Pd in it. Thus, the FWHM of the LSPR peak ($\Delta\lambda$) is directly proportional to the size (d) of the Pd NPs. For larger-sized NPs, the mean free path of the metal electrons is smaller than the size of the NPs, which leads to modification in the free-electron contribution to the dielectric function, causing the SPR peak to increase in intensity and decrease in width with increasing particle size [30]. In the present study, the NPs size was increased with the increase in the concentration of Pd in the carbon matrix [23]. However, the magnitude of change in the size of Pd NPs with the increase in concentration was not so large. Additionally, the number of free electrons in the nano-composite system also increased with the increase in the Pd concentration. Therefore, the combined effect of an increase in the size and number of free electrons leads to an increase in the intensity of LSPR, and decrease in the FWHM of LSPR peak corresponding to the increase in the Pd concentration. The effect of Pd concentration on the LSPR peak position was observed in samples annealed at 300 °C. This suggests that the position of the LSPR peak is manly depending upon the size of NPs. Since the change in size with the increase in Pd concentration was not significant, the position of the SPR peak therefore did not change.

When the annealing temperature was increased from 300 °C to 500 °C, the blue shift of 9 nm and 22 nm was observed in the absorption band at 375 nm and 500 nm. The generalized Mie scattering calculation for Pd dimer showed that LSPR peak position also depends on the separation among the NPs, and blue shift was observed with the increased NPs separation [31]. The TEM images clearly showed that inter-particle separation and the density of bigger sized NPs increased with the increase in annealing temperature. Thus, blue shifts in the LSPR peak position could be attributed to the formation of larger-sized particles and the decrease in the inter-particle coupling, due to larger separation at higher annealing temperature. In addition, the change in the NP-matrix interface as observed in TEM images could also be responsible for the blue shift. When annealing temperature was further increased to the 600 °C, a continuous film was formed, as confirmed from the XRD analysis.

4. CONCLUSIONS

In summary, atom beam sputtering was employed for the deposition of well-separated Pd nanoparticles with different concentrations in the carbon matrix. The NP size and NPs-matrix interface was modified by high temperature annealing. The as-prepared Pd NPs exhibited a Mie scattering profile and the effect of Pd concentration variation was insignificant. The position of the LSPR peak was tailored by varying the annealing temperature and was explained on the basis of the growth in the NPs size, increase in NPs separation, and modification in the NP-matrix interface. The intensity of LSPR increased and its width decreased with an increase in the Pd concentration, due to growth in size and increase in the number of free electrons. The width of the LSPR peak was affected by the modification of the Pd/C interface, which was higher for the rough interface. The LSPR properties of the Pd in the visible region can be tuned by controlling the concentration in the matrix and subsequent annealing, providing a novel material for applications in photo thermal therapy, monitoring the catalytic reaction, and optical sensors.

Highlights

1. The effects of metal concentration and annealing temperature on the localized surface plasmon resonance (LSPR) properties of Pd nanoparticles dispersed in carbon were investigated.
2. The UV-vis spectroscopy studies on as-prepared films displayed a Mie scattering profile, but not-well defined LSPR bands for all the values of Pd concentration were observed.
3. Three broad LSPR absorption bands in the visible region, along with a sharp peak at 210 nm, were observed upon annealing.
4. TEM studies displayed agglomeration and growth of NPs upon annealing.

Acknowledgment: The author (P. K. Kulriya) gratefully acknowledges the financial support by the Science and Engineering Research Board, Department of Science and Technology, Govt. of India, under project DST fast track young scientist scheme (No. SR/FT/CS-120/2011).

References and Notes

1. Huang, X., Tang, S., Mu, X., Dai, Y., Chen, G., Zhou, Z., Ruan, F., Yang, Z. and Zheng, N., **2011**. Freestanding palladium nanosheets with plasmonic and catalytic properties. *Nature Nanotechnology, 6*(1), pp.28–32.

2. Stewart, M.E., Anderton, C.R., Thompson, L.B., Maria, J., Gray, S.K., Rogers, J.A. and Nuzzo, R.G., **2008**. Nanostructured plasmonic sensors. *Chemical Reviews, 108*(2), pp.494–521.
3. Pakizeh, T., Langhammer, C., Zoric, I., Apell, P. and Kall, M., **2009**. Intrinsic fano interference of localized plasmons in Pd nanoparticles. *Nano Letters, 9*(2), pp.882–886.
4. Underwood, S. and Mulvaney, P., **1994**. Effect of the solution refractive index on the color of gold colloids. *Langmuir, 10*(10), pp.3427–3430.
5. Mulvaney, P., **1996**. Surface plasmon spectroscopy of nanosized metal particles. *Langmuir, 12*(3), pp.788–800.
6. Moores, A. and Goettmann, F., **2006**. The plasmon band in noble metal nanoparticles: An introduction to theory and applications. *New Journal of Chemistry, 30*(8), pp.1121–1132.
7. Mishra, Y.K., Avasthi, D.K., Kulriya, P.K., Singh, F., Kabiraj, D., Tripathi, A., Pivin, J.C., Bayer, I.S. and Biswas, A., **2007**. Controlled growth of gold nanoparticles induced by ion irradiation: An in situ X-ray diffraction study. *Applied Physics Letters, 90*(7), p.073110.
8. Singhal, R., Kabiraj, D., Kulriya, P.K., Pivin, J.C., Chandra, R. and Avasthi, D.K., **2013**. Blue-shifted SPR of Au nanoparticles with ordering of carbon by dense ionization and thermal treatment. *Plasmonics, 8*(2), pp.295–305.
9. Rycenga, M., Cobley, C., Zeng, J., Li, W., Moran, C., Zhang, Q., Qin, D. and Xia, Y. **2011**. Controlling the synthesis and assembly of silver nanostructures for plasmonic applications. *Chemical Review, 111*(6), pp.3669–3712.
10. Xiong, Y., Chen, J., Wiley, B., Xia, Y., Yin, Y. and Li, Z.Y., **2005**. Size-dependence of surface plasmon resonance and oxidation for Pd nanocubes synthesized via a seed etching process. *Nano Letters, 5*(7), pp.1237–1242.
11. Creighton, J.A. and Eadon, D.G., **1991**. Ultraviolet–visible absorption spectra of the colloidal metallic elements. *Journal of Chemical Society Faraday Transactions, 87*(24), pp.3881–3891.
12. Xiong, Y., Washio, I., Chen, J., Cai, H., Li, Z.Y. and Xia, Y., **2006**. Poly(vinyl pyrrolidone): A dual functional reductant and stabilizer for the facile synthesis of noble metal nanoplates in aqueous solutions. *Langmuir, 22*(20), pp.8563–8570.
13. Shen, X., Wang, G., Hong, X. and Zhu, W., **2009**. Shape-controlled synthesis of palladium nanoparticles and their SPR/SERS properties. *Chinese Journal of chemical physics, 22*(4), pp.440–446.
14. Xiong, Y., McLellan, J., Chen, J., Yin, Y., Li, Z. and Xia, Y., **2005**. Kinetically controlled synthesis of triangular and hexagonal nanoplates of palladium and their SPR/SERS properties. *Journal of American chemical society, 127*(48), pp.17118–17127.
15. Xiong, Y., Wiley, B., Chen, J., Li, Z., Yin, Y. and Xia, Y., **2005**. Corrosion-based synthesis of single-crystal Pd nanoboxes and nanocages and their surface plasmon properties. *Angewandte Chemie International Edition, 44*(48), pp.7913–7917.
16. Chen, J., Wiley, B., McLellan, J., Xiong, Y., Li, Z-Y. and Xia, Y., **2005**. Optical properties of Pd-Ag and Pt-Ag nanoboxes synthesized via galvanic replacement reactions. *Nano Letters, 5*(10), pp.2058–2062.
17. Kundu, S., Wang, K., Lau, S. and Liang, H., **2010**. Photochemical synthesis of shape-selective palladium nanocubes in aqueous solution. *Journal of Nanoparticle Research, 12*(8), pp.2799–2811.
18. Li, Yi, Yan, Y., Li, Y., Zhang, H., Li, D. and Yang, D., **2015**. Size-controlled synthesis of Pd nanosheets for tunable plasmonic properties. *Cryst. Eng. Comm., 17*(8), pp.1833–1838.
19. Yang, W.H., Schatz, G.C. and Duyne, R.P.V., **1995**. Discrete dipole approximation for calculating extinction and Raman intensities for small particles with arbitrary shapes. *Journal of Chemical Physics, 103*(3), pp.869–875.
20. Sosa, I.O., Noguez, C. and Barrera, R.G., **2003**. Optical properties of metal nanoparticles with arbitrary shapes. *The Journal of Physical Chemistry B, 107*(26), pp.6269–6275.
21. Kelly, K.L., Coronado, E., Zhao, L.L. and Schatz, G.C., **2003**. The optical properties of metal nanoparticles: The influence of size, shape, and dielectric environment. *The Journal of Physical Chemistry B, 107*(3), pp.668–677.
22. Kabiraj, D., Abhilash, S.R., Vanmarcke, L., Cinausero, N., Pivin, J.C. and Avasthi, D.K., **2006**. Atom beam sputtering setup for growth of metal particles in silica. *Nuclear Instruments and Methods in Physics Research Section B beam interactions with materials and atoms, 244*(1), pp.100–104.
23. Kulriya, P.K., Mehta, B.R., Agarwal, D.C., Kumar, P., Shivaprasad, S.M., Pivin, J.C. and Avasthi, D.K., **2012**. Giant enhancement in ferromagnetic properties of Pd nanoparticle induced by intentionally created defects. *Journal of Applied Physics, 112*(1), p.014318.
24. Kulriya, P.K., Mehta, B.R., Avasthi, D.K., Agarwal, D.C., Thakur, P., Brookes, N.B., Chawla, A.K. and Chandra, R., **2010**. Enhancement of ferromagnetism in Pd nanoparticle by swift heavy, ion irradiation. *Applied Physics Letters, 96*(5), p.053103.
25. Ghosh, S.K. and Pal, T., **2007**. Interparticle coupling effect on the surface plasmon resonance of gold nanoparticles: From theory to applications. *Chemical Reviews, 107*(11), pp.4797–4862.
26. Chen, S., Huang, K. and Stearns, J.A., **2000**. Alkanethiolate-protected palladium nanoparticles. *Chemistry of Materials, 12*(2), pp.540–547.
27. Cong-Wen, X., Cheng-Min, S., Zhi-Chuan, X., Tian-Zhong, Y. and Hong-Jun, G., **2008**. Anomalous aggregation growth of palladium nanosphere with SPR band in visible range. *Chinese Physics B, 17*(8), pp.2066–2071.
28. Jensen, T., Lelly, L., Lazarides, A. and Schatz, G.C., **1999**. Electrodynamics of noble metal nanoparticles and nanoparticle clusters. *Journal of cluster Science, 10*(2), pp.295–317.
29. Doyle, W.T., **1958**. Absorption of light by colloids in alkali halide crystals. *Physical Review, 111*(4), pp.1067–1072.
30. Zhao, J.P., Lu, M., Chen, Z.Y. and Rabalais, J.W., **2002**. Surface-plasmon-resonance-induced absorption of a metal–oxide nanoparticle composite. *Applied Physics Letters, 80*(19), p.3626.
31. Raun, F.X., Zhang, S.P., Li, Z., Yang, Z., Wu, D., Ren, B. and Xu, H.X., **2010**. Near-field coupling and SERS effects of palladium nanoparticle dimers. *Chinese Science Bulletin, 55*(26), pp.2930–2036.

Received: 30 April 2019. Accepted: 19 May 2019.